Particle Flow Model for Diffraction and Its Experimental Verification

Lai Jiankun
Sichuan College of Nursing
*Correspondence: ljk1977@qq.com

Abstract: To explore the evolutionary law between single-filament diffraction fringes and double-slit diffraction fringes, a self-made experimental device with dynamically and symmetrically adjustable slit widths was adopted to carry out comparative laser diffraction experiments. (Background) Single-filament and double-slit diffraction have long lacked a unified particle-based theoretical framework to explain fringe evolution[1][2][3][4][5]. (Methods) Self-adjustable double-slit equipment and three sets of comparative optical experiments were designed, together with a complete set of dynamic mathematical derivation based on near-field electromagnetic gradient force. (Results) The experimental results show that double-slit diffraction fringes can be continuously evolved from single-filament diffraction fringes, and both have the structural characteristics of enveloping fine fringes. The particle flow model derived in this paper can uniformly explain the diffraction laws of photons and electrons, which is highly consistent with measured data. (Conclusions) This particle-trajectory interpretation provides a new theoretical perspective for basic optical experiment teaching and diffraction mechanism research. Based on the local near-field interaction characteristics of microscopic particles, a particle flow model with particle trajectory deflection is established. Starting from the action mechanism of near-field electromagnetic gradient force, a complete set of mathematical and physical relational expressions for particle deflection angle, transverse momentum increment and diffraction fringe spacing are derived. Model parameter calibration and self-consistency test are completed by using measured experimental data. Two groups of differentiated comparative experiments prove that microscopic particles have definite propagation paths when passing through obstacles. The established particle flow model can coherently explain the diffraction imaging laws of photons and electrons uniformly, and is highly consistent with the measured fringe changes. It can provide new reference ideas and theoretical interpretation perspectives for the research on physical mechanism of diffraction and physics experiment teaching.
Keywords: Photon diffraction; Near-field gradient force; Particle flow model; Fringe evolution; Experimental calibration

1. Introduction

Single-filament diffraction and double-slit diffraction are classic research contents in wave optics and modern physics experiments. The morphological correlation and formation mechanism of the two types of diffraction fringes have always been the key points of research and teaching in fundamental physics. Traditional diffraction theories[1] interpret fringe formation from the perspective of wave coherent superposition and have been widely adopted in engineering applications and conventional teaching.

In this paper, an improved self-made double-slit experimental device is used to realize the continuous and symmetric adjustment of slit width. The whole evolutionary process from single-filament diffraction to double-slit diffraction is observed in experiments. It is found that the change of slit width causes regular gradual changes in fringe spacing, morphology and nested structure, showing an obvious internal evolutionary correlation.

Based on the particle nature of microscopic particles and the quantum near-field electromagnetic interaction effect at the edge of obstacles, this paper constructs a particle flow model, and analyzes the unified formation mechanism of single-filament diffraction and double-slit diffraction from the perspective of particle trajectory deflection induced by near-field transverse gradient force. Through the establishment of dynamic and geometric projection relational expressions[2], the theoretical derivation and experimental parameter calibration are completed, and multiple groups of comparative experiments are designed to verify the inferences. The research results provide a particle trajectory perspective different from classical wave interpretation for diffraction phenomena, enrich the research dimensions of fundamental physics diffraction mechanism, and also provide referential theoretical and experimental basis for college physics experiment teaching and intuitive understanding of diffraction rules.

2. Experiment 1: Double-slit Experiment with Dynamically Adjustable Symmetric Slit Width

2.1. Experimental Apparatus

Laser light source, double-slit experimental instrument with dynamically adjustable left and right slit widths.

The device is mainly composed of a bidirectional screw, left and right baffles and a central filament. The left and right baffles are connected by a bidirectional screw to form a single slit with adjustable width. A thin filament is placed at the center of the single slit to divide it into two equal slits. A reduction gear set is connected between the control handle and the bidirectional screw, and the whole device is fixed by a frame. Rotating the handle can dynamically and symmetrically change the width of the left and right slits.

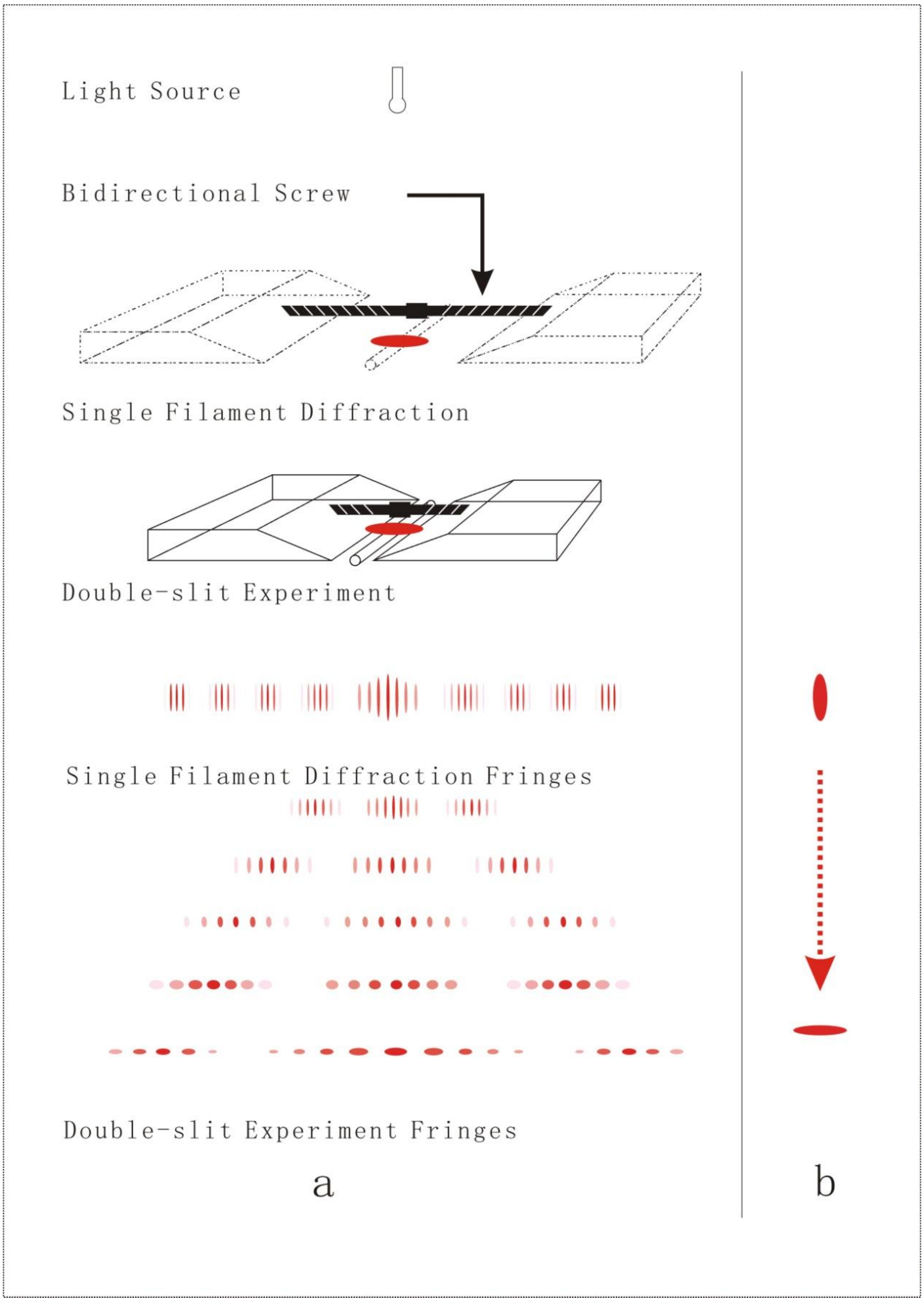

Figure 1. Schematic diagram of experimental principleFigure

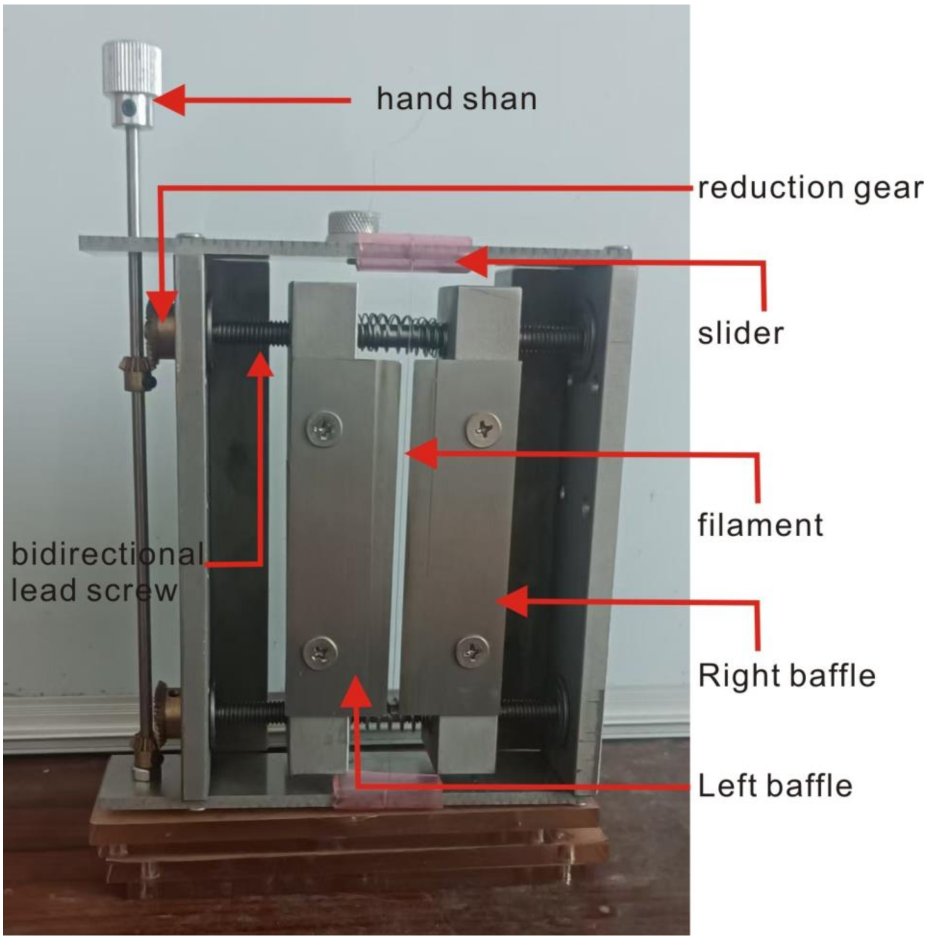

Figure 2. Physical photo of the experimental deviceFigure

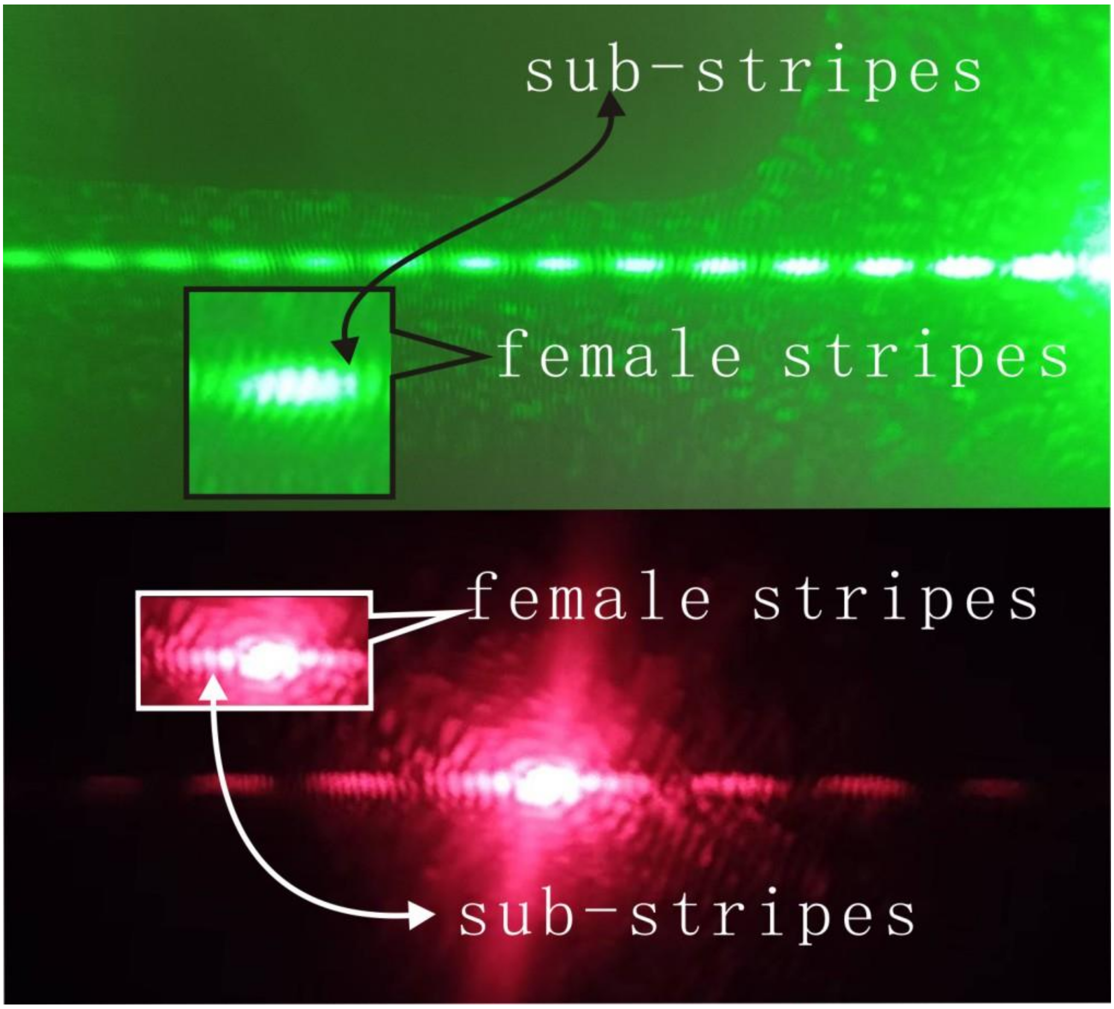

Figure3. Photograph of single-filament diffraction fringesFigure

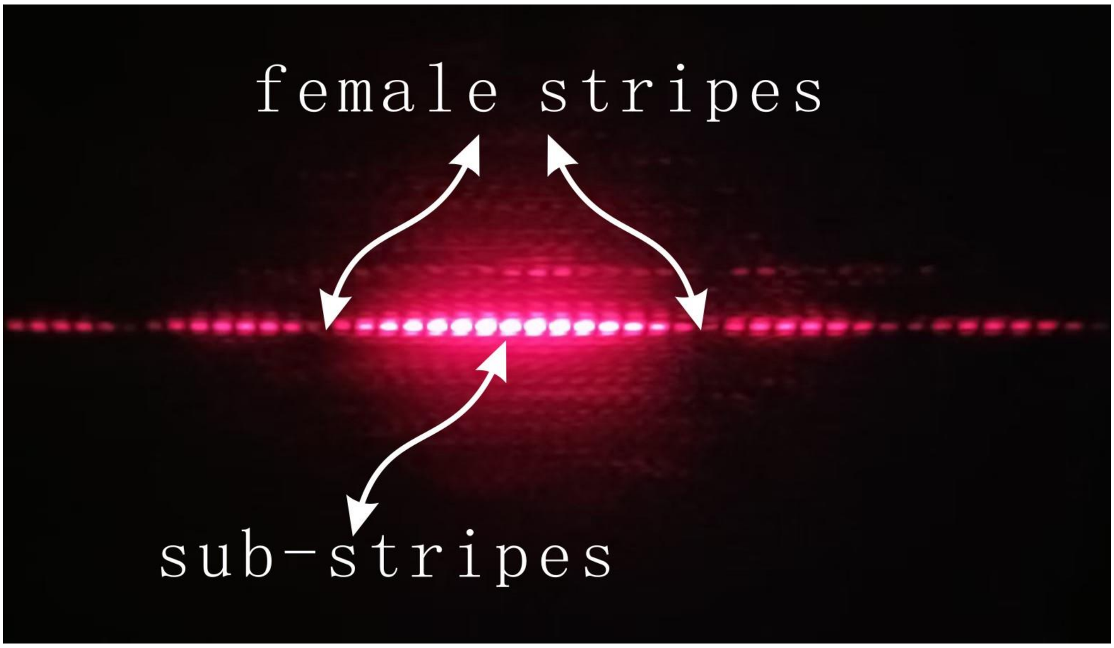

Figure 4. Double-slit diffraction fringe imageFigure

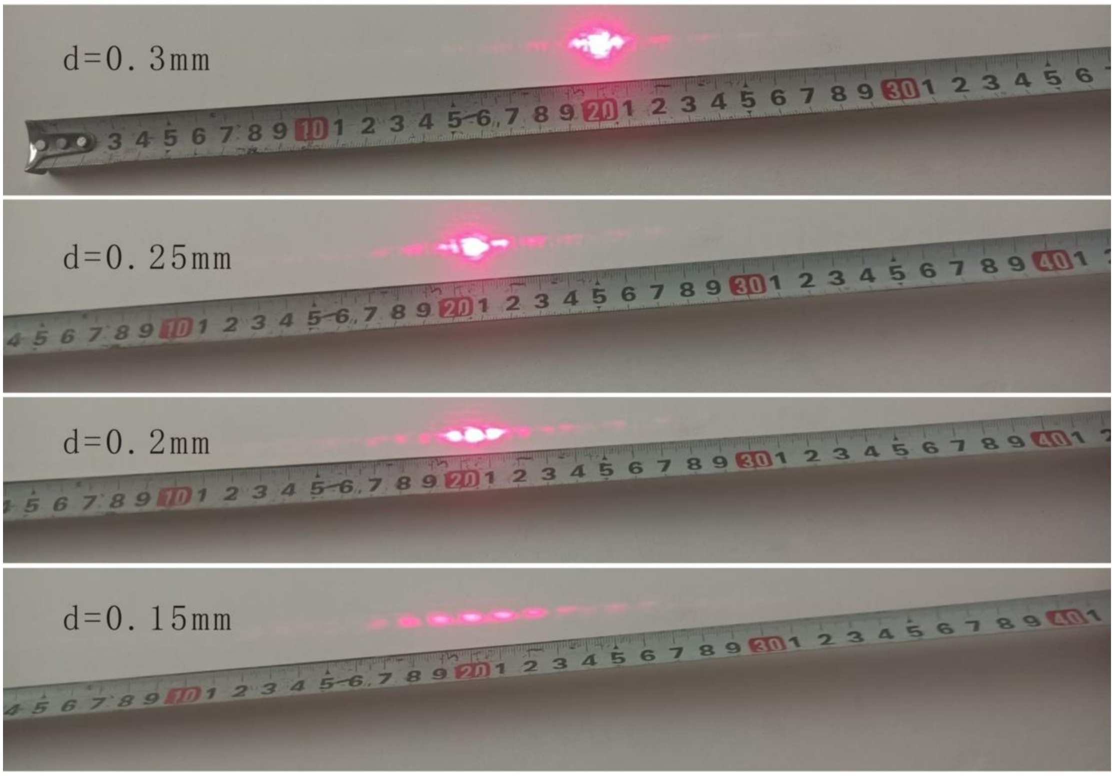

Figure 5. Sequence of fringe changes under symmetrically reduced slit width

2.2. Experimental Method

The laser irradiates the center of the double slit vertically, and the initial slit width is set to 10 mm, and only single-filament diffraction fringes are generated on the central filament. The slit width is reduced symmetrically until double-slit fringes are formed, and the changes of fringes are observed.

2.3. Experimental Results

In the slit width range from 10 mm down to approximately 0.3 mm, only single-filament diffraction fringes are observed, featuring an overall nested structure consisting of multiple groups of primary fringes enveloping secondary fringes (Figure 3), with a highly bright central fringe. As the slit width decreases from 0.3 mm to 0.15 mm, the fringes stretch outwards and their spacing increases, accompanied by homogenized brightness, eventually evolving into double-slit diffraction fringes (Figures 4, Table 1). Notably, the double-slit fringes retain the nested structural characteristics inherited from single-filament diffraction. Throughout this dynamic transition, the secondary fringes deform from thin vertical olive shapes into wide horizontal olive profiles (Figure 1b).

During the single-filament diffraction regime, the bright central secondary fringes gradually dim with expanding spacing and finally evolve into uniformly bright double-slit fringes. New secondary fringes continuously emerge on both sides of the zero-order primary fringe, increasing the total number of sub-fringes. A distinctive seesaw variation is observed among the secondary fringes that constitute the first-order primary fringe, and the centroid of the first-order primary fringe shifts outward accordingly.

2.4. Inference of Experiment 1

Double-slit fringes evolve from single-filament diffraction fringes, and clarifying the formation mechanism of single-filament diffraction is the key to explaining double-slit diffraction. When electrons approach the surface of the filament, they are subjected to Coulomb repulsion and quantum exchange forces from the surface electron cloud[3]. The deflection effect of photons near the edge can be attributed to electromagnetic near-field interaction.

3. Mathematical Derivation of Single-filament Diffraction

3.1. Core Definitions and Basic Hypotheses of Particle Flow Model

3.1.1. Core Physical Definitions

3.1.1.1. Near-field transverse gradient force *F*

When particles approach the edge of matter, they are subjected to transverse force generated by the atomic near-field Coulomb potential, which only exists in the near-field region[6][7].

3.1.1.2. Equivalent effective action length *L*

The path length of particles under the action of gradient force[5], which is determined by material and surface morphology.

3.1.1.3. Particle flow characteristic length *Λ*

$$\Lambda = \frac{h}{p}\text{; for photons } \Lambda = \lambda\text{; for relativistic electrons} \Lambda = \frac{h}{\gamma m_0 v}$$

3.1.1.4. Single fringe spacingΔx

The center-to-center distance between adjacent bright fringes on the far-field screen, which is a directly measured experimental quantity.

3.1.1.5. Intrinsic particle flow wavelength $\lambda_{flowintrinsic}$

The deflection scale corresponding to two minimum deflection angles of particles in the near-field action region, which is the intrinsic physical quantity of particle flow and determined only by material properties and particle momentum.

3.1.1.6. Projected particle flow wavelength $\lambda_{flowprojected}$

The transverse displacement corresponding to a complete particle flow cycle after geometric projection of intrinsic particle flow wavelength on the far-field screen, satisfying $\lambda_{flowprojected} = 2\Delta x$, which is a macroscopic observable quantity.

3.1.1.7. Critical filament diameter d_c

The maximum diameter of the filament that can produce particle flow and diffraction. When the diameter exceeds this value, the particle flow disappears and no diffraction occurs.

3.1.1.8. Single deflection angle θ

θ=∠BFE=∠EpD, corresponding to one fringe spacing, equal to half of the particle flow wavelength.

3.1.1.9. Maximum deflection angle θ_{max}

The maximum trajectory deflection angle of particles.

3.1.1.10. Number of particle flow cycles *N*

The number of particle flow cycles appearing on one side of the far-field screen.

3.1.1.11. Material intrinsic quantum coefficient *k*

It characterizes the action strength of near-field gradient force and is independent of particle properties.

3.1.1.12. Charge correction coefficient β

It corrects the strong coupling effect between charged electrons and edge Coulomb potential field, and distinguishes the particle flow intensity between photons and electrons.

3.1.1.13. Fringe contribution of filament$\Delta x_{filament}$

Fringe spacing generated by single-filament diffraction.

3.1.1.14. Fringe increment of baffle $\Delta x_{baffle(s)}$

The additional increment generated by the near-field gradient force at the baffle edge, which increases as the slit width decreases.

3.1.1.15. Gradient force of filament $F_{filament}$

3.1.1.16. Gradient force of baffle F_{baffle}

3.1.2. General Core Hypothesis

The interaction between microscopic particles and the near field of matter edge follows the quantized action correlation rule[8][9]:

$$(1)\ F \cdot L = \frac{kh}{t}$$

Dimensional verification:

L = Equivalent effective action

k = Material coefficient

Left side: $[F \cdot L] = MLT^{-2} \cdot L = ML^2T^{-2}$;

Right side: $\left[\frac{kh}{t}\right] = ML^2T^{-1} \cdot T^{-1} = ML^2T^{-2}$;

3.2. Complete Dynamic Derivation for Photons and Electrons

3.2.1. Derivation of particle travel time in near-field region

Particles pass through the near-field action region at a uniform velocity. The travel time is determined by the equivalent effective action length L and particle velocity v:

$$(2)\ t = \frac{L}{v}$$

3.2.2. Derivation of near-field transverse gradient force

Substitute Equation (2) into Equation (1) and rearrange to solve for near-field transverse gradient force F:

$$(3)\ F = \frac{khv}{L^2}$$

3.2.3. Derivation of particle transverse momentum variation

According to the impulse-momentum theorem, the impulse of resultant force equals the change of particle momentum. The single transverse momentum variation Δp generated by particles under the action of transverse gradient force is:

$$(4)\ \Delta p = F\,t = \frac{kh}{L}$$

3.2.4. Derivation of particle deflection angle

Under the far-field small-angle approximation, the particle flow deflection angle θ is determined by the ratio of transverse momentum increment to total momentum:

$$(5)\ \theta \approx tan\theta = \frac{\Delta p}{p} = \frac{k\Lambda}{L}$$

3.2.5. Derivation of far-field diffraction fringe spacing

Let D be the distance from the filament to the far-field screen. Based on geometric projection relation, the fringe spacing Δx formed by deflection angle on the screen satisfies:

$$(6)\ \Delta x = \theta D = \frac{\Delta p}{p} D = \frac{kh}{Lp} D = \frac{k\Lambda D}{L}$$

To facilitate comparison with traditional single-filament diffraction formula, define comprehensive material coefficient$\alpha = \frac{\mathrm{kd}}{\mathrm{L}}$ (d is filament diameter), then:

$$(7)\ \Delta x = \alpha \frac{\Lambda D}{d}$$

This formula has the same mathematical form as the traditional single-filament diffraction formula, and fully conforms to the experimental rules that fringe spacing changes with screen distance, particle wavelength and filament diameter d. The transverse momentum increment Δp is inversely proportional to the equivalent effective action length. The larger the equivalent effective action length is, the shorter the particle flow wavelength is, the smaller the transverse momentum increment is, and the less obvious the diffraction is.

3.2.6. Derivation of intrinsic particle flow wavelength

The intrinsic particle flow wavelength is the transverse deflection scale AB of particles in the near-field action region. Combined with near-field geometric relation $\theta^{intrinsic} = \frac{AB}{L}$ and Equation (5): $\frac{\mathrm{AB}}{\mathrm{L}} = \frac{2\Delta\mathrm{p}}{\mathrm{p}}$:

$$(8)\lambda_{flowintrinsic} = AB = 2k\Lambda$$

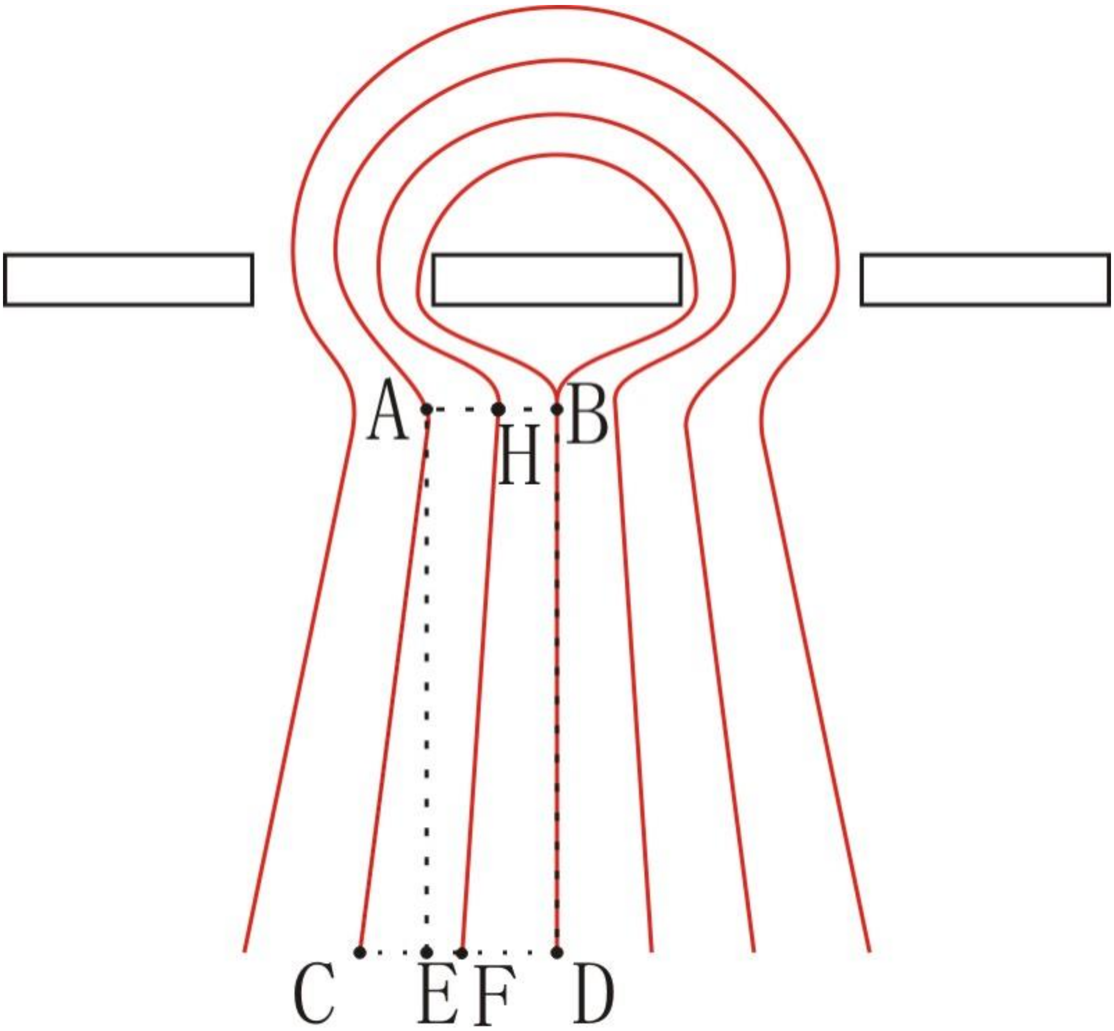

Figure 6. Schematic diagram of particle flow structure for double-slit experiment

3.2.7. Derivation of far-field projected particle flow wavelength

Combined with $\lambda_{flowprojected} = 2\Delta x$ and Equation (6):

$$(9)\lambda_{flowprojected} = CD = 2\Delta x = \frac{2k\Lambda D}{L}$$

3.2.8. Derivation of maximum deflection angle for normal incidence

$\theta = \angle BFE$ is the single deflection angle, and $\angle BpD$ is one particle flow cycle. The maximum deflection angle is the superposition of particle flow cycles on one side:

$$\theta_{max} = N \cdot 2\theta = N \cdot \frac{\lambda_{flowprojected}}{D}$$

$$(10)\theta_{max} = \frac{2Nk\Lambda}{L}$$

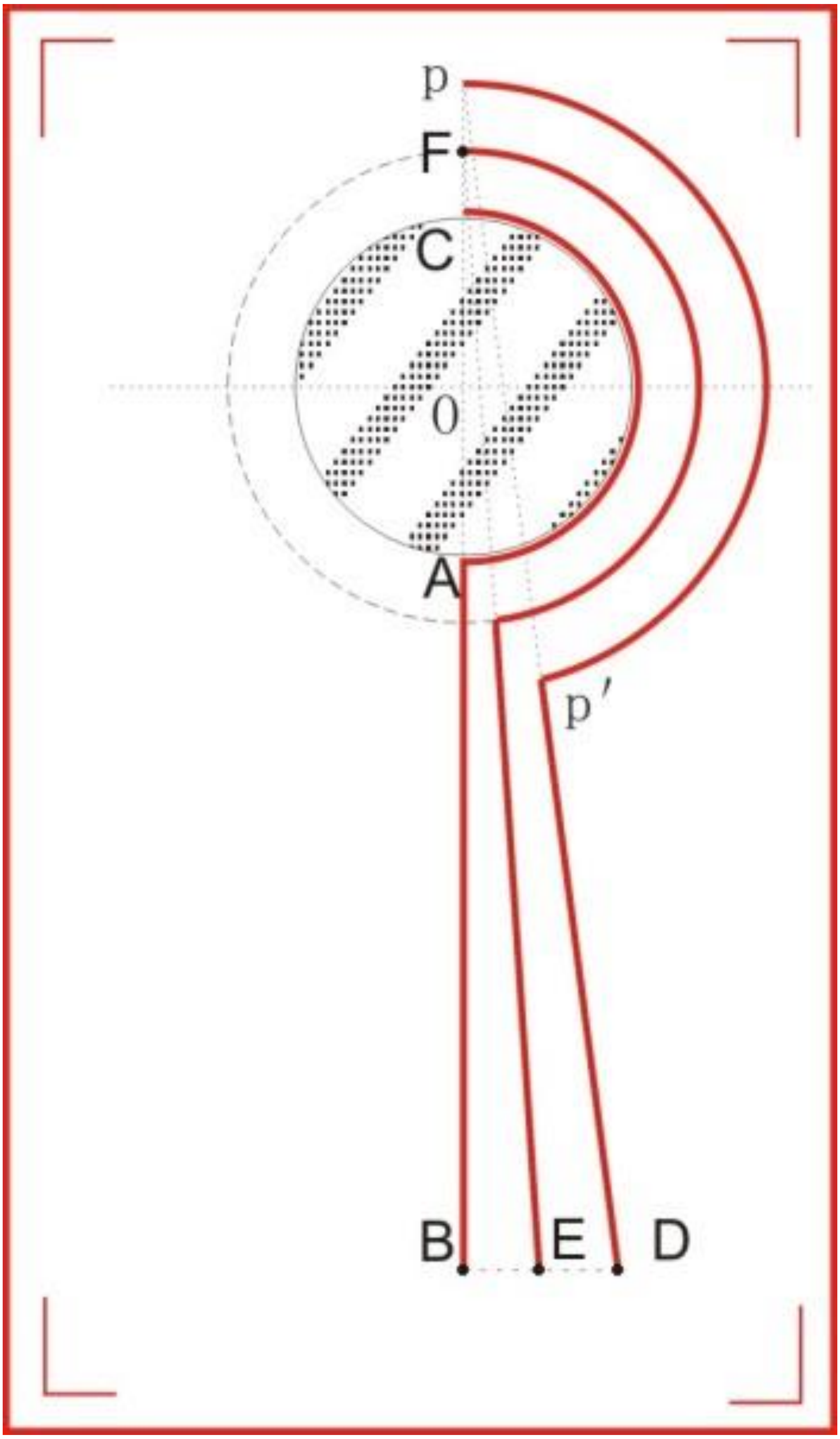

Figure 7. Geometric schematic of single-filament diffraction deflection angle

3.2.9. Derivation of maximum number of particle flow cycles

The total momentum of particle equals the product of single transverse momentum increment and total action times:

$$(11)\ N_{max} = \frac{p}{2\Delta p} = \frac{L}{2k\Lambda}$$

3.2.10. Calibration derivation of equivalent effective action length

The fringe spacing calibration method can be established by using far-field fringe spacing formula to calibrate equivalent effective action length *L* and material coefficient *k* with measured experimental parameters:

$$(12)\ \frac{k}{L} = \frac{\Delta x}{D\Lambda}$$

Where Δx is far-field single fringe spacing, Λ is photon wavelength, *D* is the distance from filament to screen.

Substitute measured data: Δx=15 mm, Λ=650×10−6 mm, D=2300 mm

$$\frac{k}{L} = \frac{15}{650 \times 10^{-6} \times 2300} = \frac{15}{1.495} \approx 10.03mm^{-1}$$

Based on near-field small-angle approximation, L≈d=0.1 mm， so

$k \approx 10.03\text{mm}^{-1}\text{L} = 1.$

Calculation Example: Given Δx=12 mm, D=2300 mm,L=0.1 mm, k≈1

$$\Lambda = \frac{L}{k}\frac{\Delta x}{D} = \frac{0.1 \times 12}{2300 \times 1} = 0.000522\ \text{mm} = 522\text{nm}$$

Note: The number of fringes observed by naked eyes in experiment is usually less than the theoretical maximum number of cycles, so it is not suitable to calibrate *L* by visual fringe counting. The fringe spacing method has stable measurement and self-consistent physics, which is the preferred method for calibrating equivalent effective action length.

3.2.11. Derivation of electron particle flow and cycle number with charge correction

Electrons have stronger coupling with Coulomb potential field at edge due to electrification. The charge correction coefficient β is introduced for single transverse momentum variation:

$$(13)\ \Delta p_e = \beta \frac{kh}{L}$$

Substitute $N_{max} \cdot 2\Delta p = p$ to get the theoretical maximum number of cycles for electrons:

$$(14)\ N_{max,e} = \frac{L}{2\beta k\Lambda}$$

Far-field fringe spacing formula for electron:

$$(15)\ \Delta x_e = \frac{\beta k\Lambda D}{L}$$

3.2.12. Derivation of critical filament diameter

The total momentum of particle is limited, so the maximum equivalent effective action length L_{max} is fixed. Larger filament diameter leads to larger equivalent effective action length provided by edge near-field. When $L = L_{max}$, only one particle flow cycle can be generated. Combined with $\lambda_{flowintrinsic} = AB = 2k\Lambda$ and $N_{max} = 1 = \frac{L}{2k\Lambda}$, and $L = d_c$:

$$(16)\ d_c = 2k\Lambda$$

3.3. Experimental Adaptation and Parameter Verification of Unified Model

3.3.1. Adaptation for photon diffraction

Substitute $\Lambda = \lambda$ for photons to get complete formulas for photon diffraction:

$$\Delta p = \frac{kh}{L}$$
$$\Delta x = \frac{k\Lambda D}{L}$$
$$\theta_{max} = N\frac{2k\Lambda}{L}$$

These formulas have the same mathematical form as the traditional single-filament diffraction formulas, only need to calibrate material coefficient *k* and equivalent effective action length *L*.

3.3.2. Adaptation for electron diffraction

For relativistic electrons, $\Lambda = \frac{h}{\gamma m_0 v}$. Combined with charge correction coefficientβ:

$$\Delta x_e = \frac{\beta k \Lambda D}{L}$$

$$N_{max,e} = \frac{L}{\beta k \Lambda}$$

3.3.3. Complete experimental calibration procedure

3.3.3.1. Photon benchmark calibration: Calibrate material coefficient *k* and equivalent effective action length *L* by using laser with known wavelength and measuring fringe spacing and cycle number.

3.3.3.2. Electron coefficient calibration: Calibrate charge correction coefficient β by using electron beam with known momentum under the same experimental conditions.

3.3.3.3. Critical diameter verification: Observe the critical diameter where diffraction disappears by replacing filaments with different diameters to verify independent coefficient.

3.3.3.4. Self-consistency verification: Verify the proportional relationship of all formulas by changing screen distance and particle wavelength.

4. Verification Experiments

Combined with mathematical derivation and experimental phenomena, photons and electrons[10][11][12] have definite propagation paths. Two more experiments are designed to verify this viewpoint.

4.1. Experiment 2: Asymmetric Experiment with Limit Slit Width of Double Slit

4.1.1. Experimental Apparatus

Laser light source, double-slit experimental instrument with adjustable slit width used in Experiment 1.

4.1.2. Experimental Method

Retain only one baffle and central filament, with an initial gap of 5 mm between baffle and filament. The laser irradiates the filament vertically to generate single-filament diffraction fringes. Gradually move the baffle close to the filament and observe fringe changes.

4.1.3. Experimental Results

When the gap between baffle and filament decreases from 5 mm to about 0.3 mm, the fringes remain unchanged as standard symmetric single-filament diffraction fringes. When the gap decreases from 0.3 mm to 0.15 mm, the fringes on the baffle side stretch outward and finally evolve into double-slit fringes, while the fringes on the other side have no obvious changes（Figure 8，Figure 9）.

The experiment shows that changing the gap between baffle and filament only affects photons on the adjacent side and changes their landing positions, and has little effect on photons on the other side. It proves that there is no interaction between photons on both sides of the filament. The experimental phenomena show that photons have traceable propagation paths when passing through obstacles, which can be explained from the perspective of particle trajectory evolution[3][4][5].

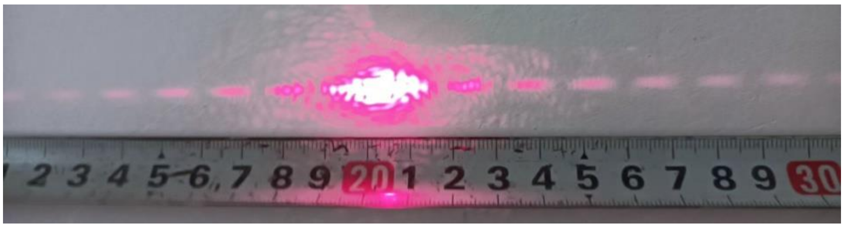

Figure 8. Fringe images with baffle－filament distance from 5 mm to 0.3 mm

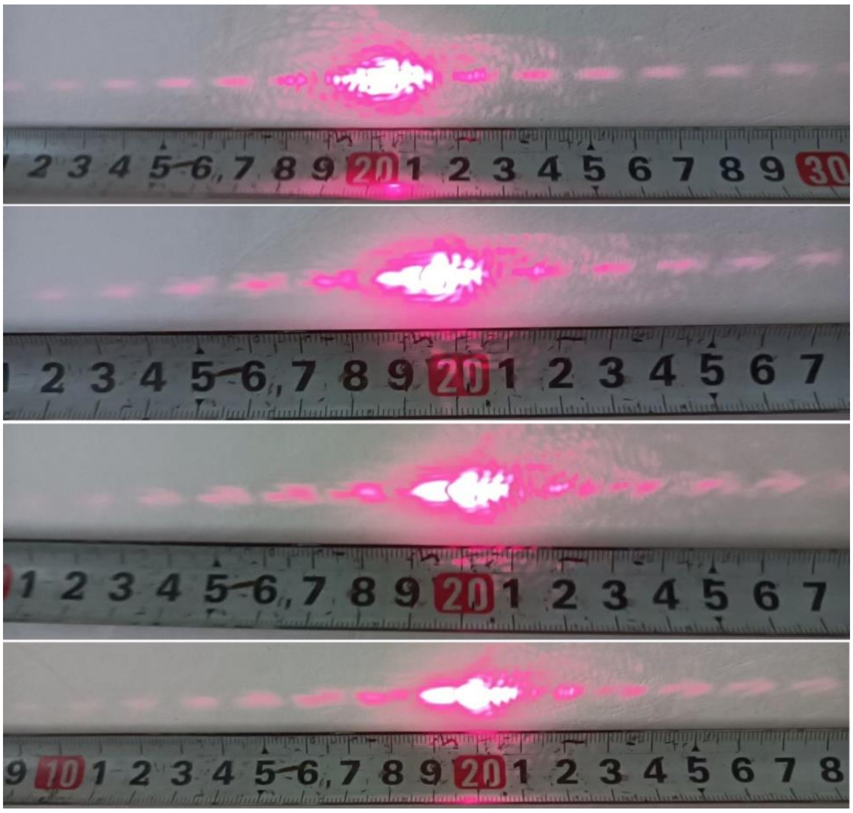

Figure 9. Fringe images with baffle - filament distance from 0.3 mm to 0.15 mm

4.2. Experiment 3

4.2.1. Experimental Apparatus

J2515 double-slit experimental instrument, color filters (thickness 0.08 mm), clean water, white light source.

4.2.2. Experimental Method

Thinner filters with similar transmittance and uniform thickness are preferred. Remove the original double slit, paste narrow color filters on two slits respectively. The joint of two filters shall be placed exactly on the middle partition without overlapping. Drop a small amount of water between filter and slit to enhance adhesion, and carry out the experiment after drying（Figure 10）.

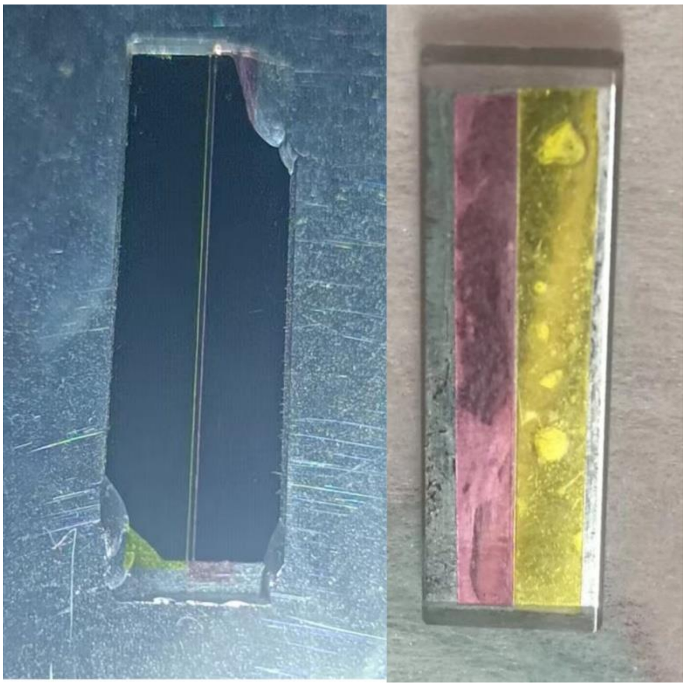

Figure 10. Double-slit device pasted with two different color filters

4.2.3. Experimental Results

Alternating bright and dark fringes are formed on the screen, and the color of each fringe is consistent with the color of the adjacent filter. The experiment clearly shows that the fringe color has one-to-one correspondence with the incident light from each slit, which reflects the ordered distribution characteristics of particle landing positions and can be described by definite trajectory model（Figure 11）.

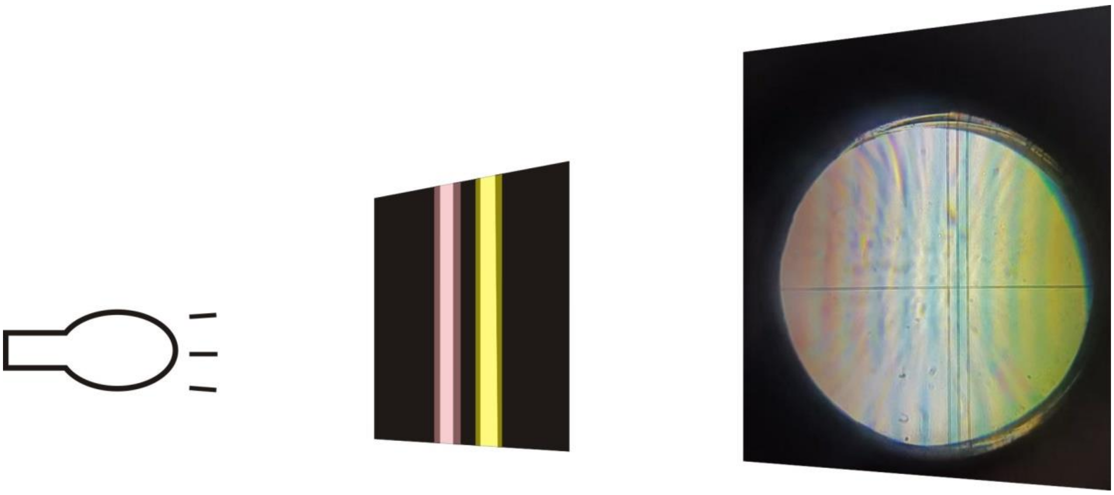

Figure 11. Diffraction fringes obtained with colored filter double slit

5. Mathematical Derivation of Double-slit Experiment

When the single-side slit width *s* changes, the total fringe spacing of double-slit is the linear superposition of fixed contribution from filament and additional contribution from baffle near-field:

$$\Delta x_{(s)} = \Delta x_{filament} + \Delta x_{baffle(s)}$$

Where *s* is slit width, $\Delta x_{filament}$ is stable fringe spacing generated by single filament (experimental value about 2.3 mm), $\Delta x_{baffle(s)}$ is additional increment generated by near-field gradient force at baffle edge, which increases as the slit width decreases.

When s≥0.3mm, the baffle is far away and $\Delta x_{baffle(s)} \approx 0$, so fringe spacing keeps constant. When 0.15 mm≤s<0.3 mm, the baffle moves close and generates outward force, leading to rapid increase of $\Delta x_{baffle(s)}$ and enlarged total fringe spacing.

6. Discussion

In Experiment 1, we observed that the bright central secondary fringes gradually dimmed with increased fringe spacing. A reasonable interpretation for this phenomenon is that photons undergo positional shifts under the near-field gradient forces generated by the filament and baffles, transferring from the upper-order secondary fringes to the lower-order ones. The rise and fall of photon quantities manifest as variations in fringe brightness, resulting in the seesaw pattern of secondary fringes and the morphological transformation from vertical olive-shaped sub-fringes to horizontal ones (Figure 12).

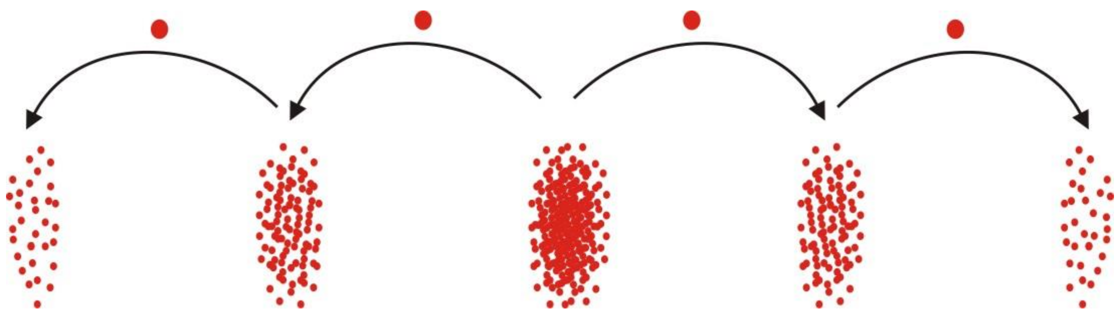

Figure 12. Schematic diagram of stepwise photon migration

The phenomena of Experiment 2 and Experiment 3 are consistent with mathematical derivation, proving that photons have traceable propagation paths when passing through obstacles. A large number of particles form consistent trajectories under the action of the same obstacle and generate particle flow around the obstacle. After passing the obstacle, particles gather at crests and troughs of particle flow without new obstacles to break the dynamic balance. As discrete particles, photons and electrons propagate linearly along the tangent direction of crests and troughs, and finally form bright fringes on the screen. Few particles arrive between crests and troughs, forming dark fringes, so alternating bright and dark fringes appear instead of a single bright spot or line（Figure 13）.

At the far end of fringes, the amplitude of particle flow gradually decreases, crests and troughs merge with each other, and bright and dark fringes evolve into a continuous bright line. Human eyes are most sensitive to green light, so a continuous bright line can be observed at the far field in single-filament diffraction experiment using green laser.

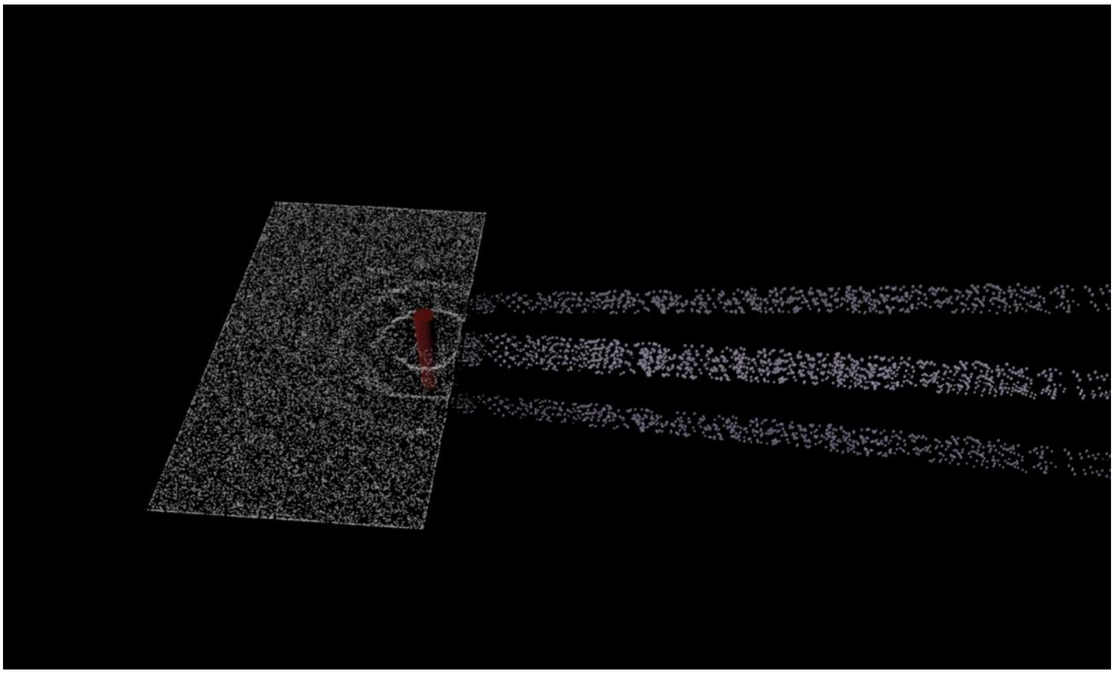

Figure 13. 3D schematic of single-filament particle flow field

6.1. Crucial Phenomenon Comparison

According to traditional wave theory, alternating bright and dark fringes gradually fade and disappear at the far field without forming a continuous bright line.

According to particle flow model, the amplitude of particle flow decreases at the far field, crests and troughs merge, and alternating fringes evolve into a continuous bright line, which is consistent with experimental observation.

7. Conclusions

Diffraction is a physical phenomenon in which microscopic particles deflect under the effect of quantized near-field electromagnetic gradient forces when approaching material surfaces. This phenomenon is a localized physical effect between substances with a definite range of action. Although the formula for the wavelength of particle flow resembles that derived from wave theory, the two differ fundamentally in their physical interaction mechanisms and interpretative perspectives. The flow-around theory is derived based on the interactions between particles.

8. Experimental Data

8.1. Table 1: Relationship between slit width and measured fringe spacing

Slit width *s* (mm)	Measured fringe spacing Δx (mm)
0.15	10.6
0.20	8.3
0.25	5.8
0.30	2.8
0.35–1.00	2.3

Table 1 shows that when the slit width is greater than about 0.3 mm, photons are far away from the baffle and not affected by the near-field force of baffle, only affected by the near-field force of filament, forming stable single-filament diffraction fringes. When the baffle moves close to the filament, the near-field force of baffle gradually acts on photons. At this time, photons are affected by both filament force F_{filament} and baffle force F_{baffle}. The two forces are opposite in direction, so the fringe spacing increases obviously when the slit width ranges from 0.3 mm to 0.15 mm.

Data 1: Δx=15 mm, Λ=650×10−6 mm, D=2300 mm, d=0.1 mm

Data 2: Δx=12 mm, D=2300 mm, d=0.1 mm

References

[1] Yang, K.Y.; Wei, W.L.; Ma, X.F.; Chen, B.T.; Chu, J.Q.; Liu, X.L.; Cheng, Y.H.; Yang, H.; Ma, H.T.; Qi, B.; Xie, Z.L. Disentanglement of mixed interference fringes. arXiv Preprint arXiv:2404.06716, 2024. https://doi.org/10.48550/arXiv.2404.06716.

[2] Feynman R, Leighton R and Sands M 2010 The Feynman Lectures on Physics v. 3 (New York, USA: Basic books) ISBN 9780201021189

[3] Liu, XJ., Miao, Q., Gel'mukhanov, F. et al. Einstein–Bohr recoiling double-slit gedanken experiment performed at the molecular level. Nature Photon 9, 120–125 (2015). https://doi.org/10.1038/nphoton.2014.289

[4] Harada, K., Akashi, T., Niitsu, K. et al. Interference experiment with asymmetric double slit by using 1.2-MV field emission transmission electron microscope. Sci Rep 8, 1008 (2018). https://doi.org/10.1038/s41598-018-19380-4

[5] Tavabi, A.H., Boothroyd, C.B., Yücelen, E. et al. The Young-Feynman controlled double-slit electron interference experiment. Sci Rep 9, 10458 (2019). https://doi.org/10.1038/s41598-019-43323-2

[6] Engay, E., Shanei, M., Mylnikov, V. *et al.* Transverse optical gradient force in untethered rotating metaspinners. *Light Sci Appl* **14**, 38 (2025). https://doi.org/10.1038/s41377-024-01720-x

[7] Huang, F., Ananth Tamma, V., Mardy, Z. *et al.* Imaging Nanoscale Electromagnetic Near-Field Distributions Using Optical Forces. *Sci Rep* **5**, 10610 (2015). https://doi.org/10.1038/srep10610

[8] Lu, J.S.; Ginis, V.; Lim, S.W.D.; Capasso, F. Helicity and Polarization Gradient Optical Trapping in Evanescent Fields. Phys. Rev. Lett. 2023, 131, 143803. https://doi.org/10.1103/PhysRevLett.131.143803

[9] Kings-Smith, J.J.; Picardi, M.F.; Wei, L.; Zayats, A.V.; Rodríguez-Fortuño, F.J. Optical forces from near-field directionalities in planar structures. arXiv Preprint arXiv:1811.05237, 2018. https://doi.org/10.48550/arXiv.1811.05237

[10] Mahmoudi, S., Gruene, T., Schröder, C. *et al.* Experimental determination of partial charges with electron diffraction. *Nature* **645**, 88–94 (2025). https://doi.org/10.1038/s41586-025-09405-0

[11] Esat, T., Friedrich, N., Tautz, F.S. et al. A standing molecule as a single-electron field emitter. Nature 558, 573–576 (2018). https://doi.org/10.1038/s41586-018-0223-y

[12] Wong, L.J., Rivera, N., Murdia, C. *et al.* Control of quantum electrodynamical processes by shaping electron wavepackets. *Nat Commun* **12**, 1700 (2021). https://doi.org/10.1038/s41467-021-21367-1

Author Contributions

Conceptualization, Lai J.K.; methodology, Lai J.K.; validation, Lai J.K.; formal analysis, Lai J.K.; investigation, Lai J.K.; data curation, Lai J.K.; writing—original draft preparation, Lai J.K.; writing—review and editing, Lai J.K.; visualization, Lai J.K. All authors have read and agreed to the published version of the manuscript.

Funding

This research received no external funding.

Institutional Review Board Statement

Not applicable. This study only involves optical laser physical experiments without human or animal subjects.

Informed Consent Statement

Not applicable.

Data Availability Statement

All experimental measurement data and mathematical calculation data generated during this study are fully included within the manuscript, and no external datasets are used.

Acknowledgments

No additional institutional or individual technical support is acknowledged.

Conflicts of Interest

The author declares no conflict of interest.